Design of Catechin-based Carbon Nanodots as Facile Staining Agents of Tumor Cells

Yaung Kwee[1,2], Alfinda Novi Kristanti[1], Nanik Siti Aminah[1], and Mochamad Zakki Fahmi[1,3,*]

[1]*Department of Chemistry, Airlangga University, Kampus C Mulyorejo, Surabaya 60115, Indonesia*

[2]*Department of Chemistry, University of Mandalay, University Drive, 73rd Mandalay, Myanmar*

[3]*Supramodification Nano-micro Engineering Laboratory, Airlangga University, Kampus C Mulyorejo, Surabaya 60115, Indonesia*

* ***Corresponding author:***

email: m.zakki.fahmi@fst.unair.ac.id

Received: October 2, 2019
Accepted: January 3, 2020

DOI: 10.22146/ijc.50327

Abstract: *Carbon nanodots (CNDs) have widely received great attention as a result of favorable optical, electrical, optoelectrical, biocompatible, and non-toxic properties that these nanoparticles possess. However, the exploration of nanoparticles from natural raw material is still limited. In the present work, carbon dots were produced from catechin isolated from* Uncaria gambir *through a simple and facile process. Carbon nanodots were produced by the pyrolysis process of catechin, which allowed it for carbonization. Owing to its unique properties, such as photoluminescence with an emission peak at 500 nm (λ_{ex} = 380 nm), average size diameter of about 5 nm and non-toxic properties, Cat-CNDs were incredibly potential for staining targeted tumor cells. The staining ability shown by confocal microscopy observations showed their green fluorescence images which meant that the CNDs easily penetrated HeLa cells via endocytosis. The resulting CNDs which were analyzed using several significant techniques proved that the prepared Cat-CNDs were tremendously dispersible and water-soluble, had good colloidal stability, excellent biocompatibility, favorable hydrophilicity, high photostability, and were non-toxic.*

Keywords: Uncaria gambir*; catechin; carbon nanodots; staining tumor cells*

■ INTRODUCTION

Gambir is one of the most important economical natural products in which Indonesia is the world's largest exporter, currently supplying 80% of the global market [1]. Moreover, it is a well-known and cost-effective plant, and considered as a promising medicinal plant that is found in Southeast Asian regions such as in West Sumatera of Indonesia and in the Peninsula of Malaysia. The family of the genus *Uncaria* is Rubiaceae, containing approximately 34 species, which abundantly grow in tropical regions of Southeast Asia, Africa, and South America [2-5]. The hooks of *Uncaria gambir* are conventionally prepared for the treatment of wounds, ulcers, fever, asthma, rheumatism, hyperpyrexia, hypertension, headaches, gastrointestinal illness, and bacterial or fungal infections [6-9]. Catechin, a polyphenolic compound, can be isolated from *Uncaria gambir* as a particular compound [10-11]. There have been reports on the pharmacological uses of catechin to enhance mental and behavioral symptoms of dementia that includes dementia with Lewy bodies, aggressiveness in patients with Alzheimers, agitation, hallucinations, and other forms of senile dementia [12-13].

In 2004, carbon dots (CDs) were accidentally discovered during the separation and purification of the single-walled carbon nanotubes and became a potentially new component of fluorescent carbon material with a diameter in the range of below 10 nm. Subsequently, many studies regarding the nature of CDs have been developing at a great rate [14]. Consequently, there are currently many exploratory methods for the potent fabrication of fluorescent CNDs, such as electrochemical oxidation, chemical oxidation, arc-discharge, pyrolysis method, laser ablation, hydrothermal method, and solvothermal method, which can simply be classified into top-down and bottom-up approaches [15]. However, in contrast with heavy-metal-based quantum dots, carbon nanoparticles are

considered more reliable, exhibiting great advantages such as low toxicity, good water dispersibility, favorable biocompatibility, and excellent photostability especially for several clinical applications [16-17]. Furthermore, carbon nanodots derived from natural products have received great reputation due to particular merits such as photostability, excellent biocompatibility, optoelectrical properties, additional luminescence, and non-toxic nature. In addition, specific hydrophobic sites on CDs allow the improvement of diagnostics and therapy in clinical applications [18-19].

Recently, a great deal of attention have been particularly given to the production of carbon dots (CDs/CNDs) derived from natural products since they have a large number of advantages such as being renewable and sustainable and also other advantages that have already been mentioned above, [20]. Furthermore, heteroatoms from natural products promote heteroatom-doped nanocarbon dots without the addition of any external heteroatom sources. There are many ways to synthesize carbon nanodots from natural products that are incredibly green and simple compared to conventional preparation methods of carbon quantum dots from artificial carbon sources [21]. There are many literature and reports of green carbon nanodots synthesized from organic products such as from plant extracts, fruits, leaves, fruit shells and peels, algae, and fruit juice for many applications. In contrast with past applications, carbon nanodots are currently considered to be applied in photothermal treatment, drug delivery systems, photoacoustic imaging, fluorescence imaging, sensing, and magnetic resonance imaging, and is recognized to be a beneficial eco-friendly alternative to semiconductor quantum dots [22]. Yallapa et al. reported that carbon nanodots with porous particles can be synthesized from OPL (Oil Palm Leaves) which contained several important organic products such as cellulose, lignin, and hemicelluloses. Those CNDs were conjugated with fluorescent dye for cellular imaging and targeted drug delivery to cancer cells [23]. Carbon nanodots synthesized from molecules or compounds with rigid and graphene-like structures showed strong fluorescence likely due to the presence of aromatic rings and hydroxyl groups, in which the aromatic rings were able to form co-planar structures and causing the hydroxyl group to become dehydrated and introduce oxygen defects [24]. As a promising cost-effective alternative, CNDs have recently been considered as a new quantum dot candidate. In addition, carbon nanodots synthesized from aromatic rings and abundant hydroxyl groups also have benefits of better surface grafting, stable photoluminescence, good solubility, and low toxicity, and thus making them promising materials [25-27].

There are several commonly used treatment methods for cancer such as chemotherapy, radiation, surgery, targeted treatments, and immunotherapy that are applied separately or in combination [28]. However, these treatment methods might bring about various side effects [29]. On the other hand, drug nanocarriers were reported to have improved cancer treatment efficacy and diminish side effects of the conventional methods [30-31]. Several studies have reported the application of CNDs on cancer treatment [32-34]. In the present study, we synthesized potential carbon nanodots (CNDs) from catechin as a natural product isolated from *Uncaria gambir*. The as-prepared nanoparticles (Cat-CNDs) from the organic product catechin has great biofunctions and can potentially be applied for staining specific tumor cells. The optimization of the synthesized Cat-CNDs was performed by characterizations of optical properties, spectroscopic properties, and bioassay tests using different analytical techniques. According to its unique properties discovered from the performed analysis, Cat-CNDs are highly expected to contribute to improving the method of cancer theranostics to a great extent. Furthermore, the synthesized Cat-CNDs are considered to be more biocompatible, have high cell uptake when diagnosing cancer cells, and great cell viability for staining specific tumor cells.

■ EXPERIMENTAL SECTION

Materials

The dried blocks of *Uncaria gambir* were collected from a commercial market in Surabaya, Indonesia. Some of the chemicals such as hydrochloric acid (97%, HCl),

sodium chloride (55.5%, NaCl), ethanol (99.9%), sodium hydroxide (98.5%, NaOH), and ethyl acetate (99.8%, EA) were purchased from Sigma-Aldrich, USA. The WST-8 reagent of [monosodium (2-(2-methoxy-4-nitrophenyl)-3-(4-nitrophenyl)-5-(2, 4-disulfophenyl) 2H-tetrazolium)] was bought from TCl, Japan. Phosphate-buffered saline (PBS) was from UniRegion, Biotech, Taiwan. All reagents were of analytical grade and used as received without any further purification.

Procedure

Isolation of catechin

The dried blocks of *Uncaria gambir* (350 g) were ground into fine powders using a mortar and pestle. To attain the uniform-sized raw powders, sieving was performed at 62 μm using a laboratory sieve. The fine powders were then collected for further work. The fine powders (300 g) were extracted with methanol for 24 h and then it was further extracted three more times. The methanol extract was then evaporated in order to obtain methanol crude extract. The methanol crude extract was then partitioned three times with *n*-hexane. After that, the methanol liquid extract was partitioned again three times with ethyl acetate in order to get the ethyl acetate crude extract. The ethyl acetate extract (12 g) was taken and separated by silica gel column chromatography with a gradient of *n*-hexane in EA (50:50, 40:60, 30:70, 20:80, 10:90, 0:100). The purified catechin (7 g) was isolated from solvent ratios of *n*-hexane: EA (2:8) and the structure was further confirmed by spectroscopic techniques.

Synthesis of carbon nanodots (CNDs)

The Cat-CNDs were derived from the isolated pure catechin through a single-step method of pyrolysis following a previous report [35]. Experimentally, 50 mg of the purified catechin was powdered and placed on the isolated reactor to avoid air flow, then pyrolyzed at 250 °C for 4 h in a furnace for the carbonization process. The resulting Cat-CNDs were dissolved in 1 M NaOH at 60 °C, subjected to dialysis process (MWCO 10.000 kDa) and collected by centrifugation (12.000 rpm, 2 h) for further use.

Cell culture

To culture human cervical (HeLa) tumor cells, Eagle's minimum essential medium (EMEM, containing 1.5 g L^{-1} sodium bicarbonate) was used, which was added for cell medium with the respective content of 1% of antibiotic-antimycotic formulation, 1% of non-essential amino acid, 1% of l-glutamine, 1% of sodium pyruvate, and 10% of fetal bovine serum. The cells treated were then put safely in a humidified incubator with 5% of CO_2 which was maintained at 37 °C.

Confocal imaging observation

For the exploration of the potential bioimaging and cellular distribution of Cat–CNDs, HeLa cells were implanted at a density of 5 × 104 cell mL^{-1} in 1 mL EMEM medium in 24-well plates. Hence, a newly medium containing varied and different concentrations of Cat–CNDs was attached to the corresponding dishes and was incubated for 1 h. Afterwards, the medium was washed twice with PBS and fixed with ethanol. Then, the samples were captured by using a laser scanning confocal microscopy (CLSM). CLSM images were obtained by irradiating the samples with inline Ar (488 nm) and He–Ne (503–680 nm and 588 nm) lasers.

Cytotoxicity assessment

The assessment of cell viability was evaluated using a WST-8 assay in HeLa tumor cells. HeLa cells, which were cultured in EMEM, were cultured in 24-well plates (15.000 cells per well) for 24 h. After rinsing with PBS to wash the proliferated cells and the cells were incubated with an adjusted concentration of Cat-CNDs for 24 h. After rinsing the plate twice with PBS, WST-8 reagent (1 mL, 500 mg mL^{-1}) was supplemented and incubated for 4 h. Afterwards, dimethyl sulfoxide (1 mL) was added to each well to dissolve formazan crystals, and the crystals' absorbance was determined at 570 nm using an Elisa reader (Biotech Powerwave XS). The greater the absorbance intensity, the more the number of live cells because more formazan was being absorbed.

$$\text{Cell viability} = \frac{\text{A570 in treated cell}}{\text{A570 in control sample}} \times 100\%$$

Characterization

The Nuclear Magnetic Resonance spectroscopy (NMR), Brucker Ultra shield Advance II 600 MHz was used to characterize the isolated catechin compound. Related spectroscopy methods of nuclear magnetic

resonance (NMR) such as heteronuclear single quantum coherence spectroscopy (HSQC) and heteronuclear multiple-bond coherence spectroscopy (HMBC) was also applied. Atomic force microscopic photographs were achieved using a scanning probe AFM5500M instrument (Hitachi Co., Japan) at ambient temperature. UV-Vis absorption spectra were determined using a JASCO V-670 spectrometer. By using a Rigaku 18 kW rotating anode source X-ray diffractometer with Cu Kα1 line radiation (λ = 1.54 Å), Powder X-ray diffraction (XRD) diagrams were analyzed. By using a PerkinElmer LS 55 spectrofluorometer equipped with a 20 kW xenon lamp, PL spectra were measured. Fourier transforms infrared (FTIR) spectra were observed with a Nicolet AVATAR 360 FTIR instrument. Raman analysis was performed using an MRS-320 Raman Instrument system (Horiba Ltd., Japan). Colloidal stability tests were performed in different pH (3–12), different temperatures (30–100 °C), and different concentrations of NaCl salts (0–0.5 M). All analyses were conducted at room temperature.

Statistical analysis

The statistical study, performed by determining the cytotoxic concentration that causes a 50% decrease in cell viability (IC_{50}), was conducted using dose-response mode on the nonlinear fitting curve in Origin software (version 8.0724, Origin Lab Inc., Northampton, MA). Means were calculated using a paired-sample t-test, and all presented data were achieved in triplicates.

■ RESULTS AND DISCUSSION

Extraction, Isolation, and Elucidation of Catechin

By the extraction process, the white crystals of catechin (7 g) were obtained. High purity of this compound was determined by performing a single spot analysis at R_f = 0.39 (eluent; Ethyl acetate:*n*-hexane = 8:2) and also determining its melting point at 125–126 °C. NMR analysis was conducted to confirm the catechin chemical structure (Fig. S1, supporting information). The analysis of the ^{1}H-NMR indicated the presence of nine protons (Fig. S1) with aromatic protons that indicated chemical shifts at 5.88–6.90 ppm. Besides that, non-aromatic cyclic protons exhibited chemical shifts at 4.06–4.56 ppm. The signal that appeared at 2.53–2.98 ppm corresponded to the secondary protons of methylene (-CH_2-). The aromatic protons appeared at δ_H 6.02 ppm (H_6, d, J = 2.3 Hz), δ_H 5.88 ppm (H_8, dd, J = 2.3 Hz), δH 6.90 ppm ($H_{2'}$, d, J = 2.1Hz), δ_H 6.8 ppm ($H_{5'}$, d, J = 6 Hz), and δ_H 6.76 ppm ($H_{6'}$, dd, J = 6 Hz, and J = 2.1 Hz). According to the three coupling constant values, the $H_{6'}$, $H_{5'}$, and $H_{2'}$ protons formed an ABX system on ring B, whereas H_6 was at meta position to H_8 on ring A. The non-aromatic cyclic protons appeared as a doublet at δ_H 4.56 ppm (H_2, d) and multiplet at δ_H 4.06 ppm (H_3, m). The last proton chemical shifts at δ_H 2.53 ppm (H_{4a}, dd) and δ_H 2.98 (H_{4b}, dd) were given by the secondary protons of methylene (-CH_2-).

The ^{13}C-NMR showed 15 signals which showed the number of carbons in the structure of the isolated pure catechin compound as demonstrated in Fig. S2. Through the DEPT 135 spectrum, it could be seen that the isolated compound included seven- tertiary carbons (δ_C, 68.30; 82.68; 95.38; 96.10; 115.19; 115.64 and 119.99 ppm), seven-quaternary carbons (δ_C, 100.60; 132.13; 145.60; 145.70;156.85; 157.70 and 157.17 ppm), and one-secondary carbon (δ_C 28.80).

The information about the correlation between directly-bonded ^{1}H on ^{13}C was obtained by the HMQC spectrum. Table 1 is the result of HMQC spectrum analysis. Moreover, the ^{1}H–^{1}H correlated spectroscopy (COSY) was used to analyze the correlation between proton and another proton in adjacent carbon. The correlation spectrum of ^{1}H–^{1}H COSY of isolated catechin compound was indicated in Fig. 1(a) and 1(b) as supplementary materials.

Moreover, the HMBC spectrum showed the presence of long-range correlations between protons and carbons that could be seen in Fig. 2(a) and 2(b) as supplementary material.

The spectrum data was made in contrast with the similar catechin compound which was isolated and identified from Acacia catechu Willdenow, reported by Acharya [36].

Synthesis and Characterization of Cat-CNDs

Pure catechin was used as raw materials to produce Cat-CNDs. The cyclohexane and benzene structure

owned by catechin was a basic reason for choosing this organic compound. By giving a thermal treatment at 250 °C, catechin will go through both dehydration and carbonization resulting in graphene like the structure of carbon dots as shown on Scheme 1. Thus, the preparation of Cat-CNDs was highlighted through a one-pot step method of pyrolysis.

To obtain solution form, the fabricated Cat-CNDs can be dissolved in polar solvents. The morphology of synthesized Cat-CNDs was firstly identified by the atomic force microscopy. The Cat-CNDs exhibited uniformly dispersible materials without any apparent aggregation. The diameter of Cat-CNDs supported its sizes between 2 and 5 nm (Fig. 3). The analysis of Cat-CNDs by AFM (Atomic Force Microscopy) is to assess the morphology, topography, and size distribution of the as-prepared CNDs. Fig. 3 also shows the characteristic AFM photographs of the

Table 1. ^{1}H, ^{13}C and HMBC NMR data of catechin in $CDCL_3$ (δ in ppm)

No. of Atom	δH (mult, J Hz)	δc
2	4.56, d	82.68
3	4.06, m	68.30
4	2.53, dd; 2.98, dd	28.80
10	-	100.60
5	-	157.17
6	6.02 (d, J = 2.3 Hz)	96.10
7	-	157.70
8	5.88 (dd, J = 2.3 Hz)	95.38
9	-	156.65
1’	-	132.13
2’	6.90 (d, J = 2.1 Hz)	115.19
3’	-	145.60
4’	-	147.70
5’	6.8 (d, J = 6 Hz)	115.64
6’	6.76 (dd 6.76 (dd, J = 6, & 2.1 Hz)	119.99

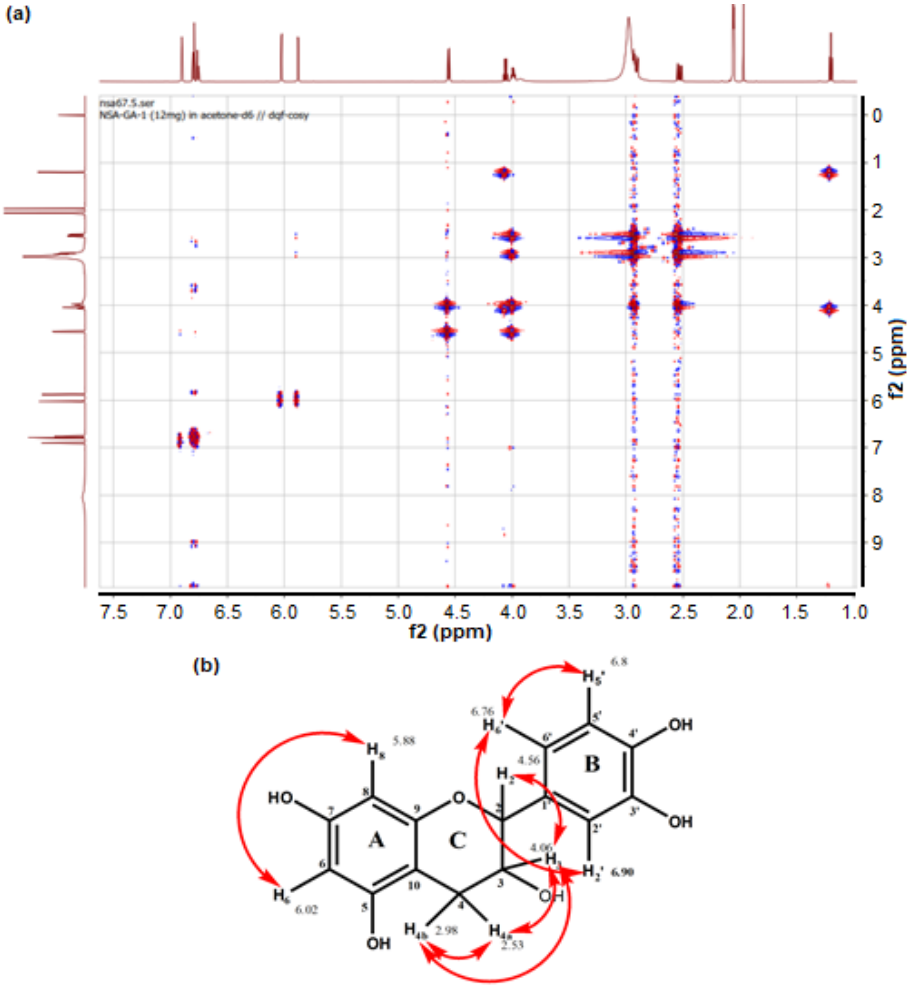

Fig 1. (a) The ^{1}H-^{1}H correlation spectrum of catechin, (b) The correlation of ^{1}H–^{1}H COSY of isolated compound

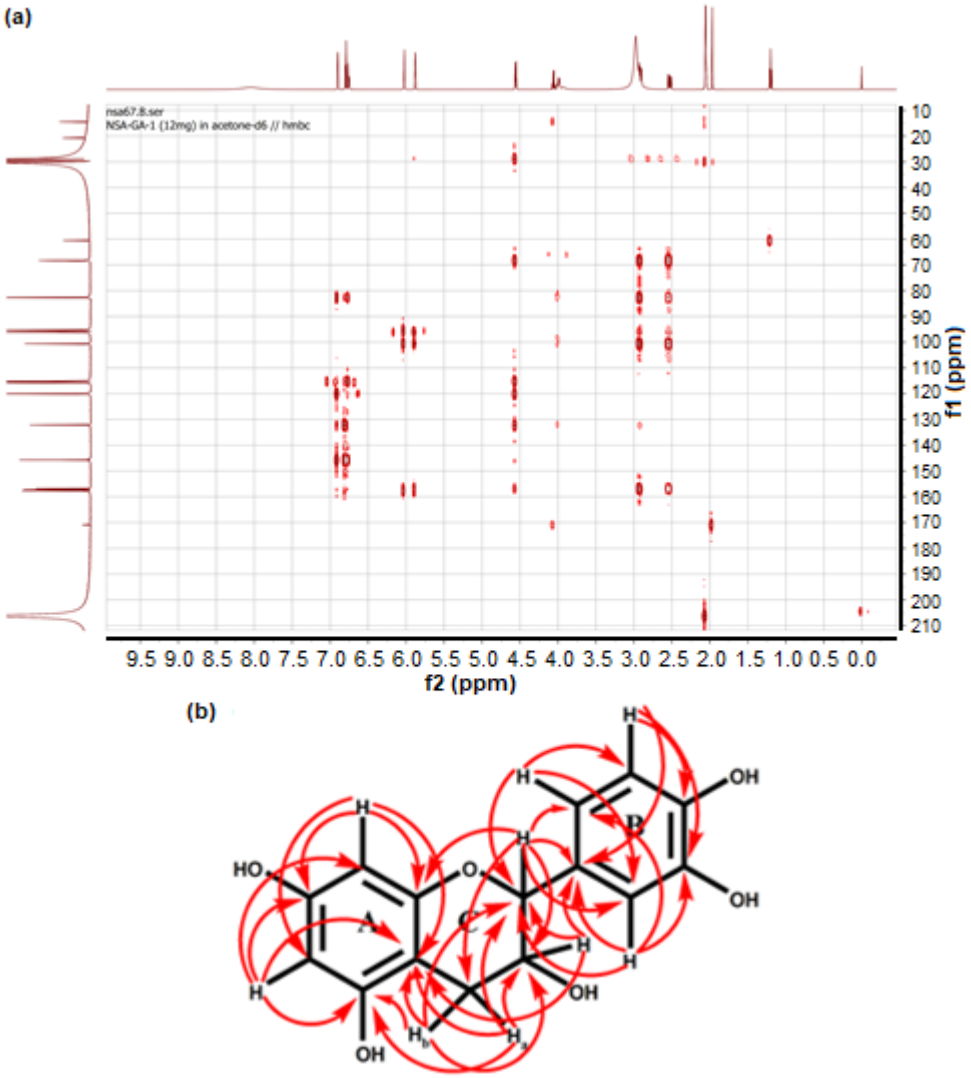

Fig 2. (a) The long-range correlation spectrum of ^{1}H-^{13}C HMBC of isolated catechin compound, (b) The correlation of HMBC in the isolated catechin compound

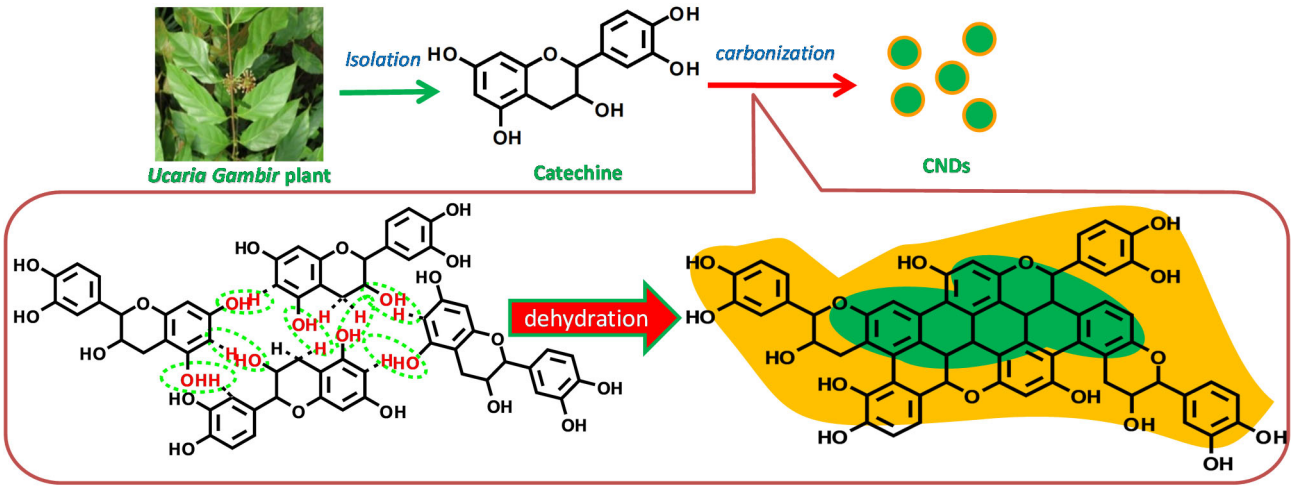

Scheme 1. Schematic illustration synthesis of Cat-CNDs from catechin

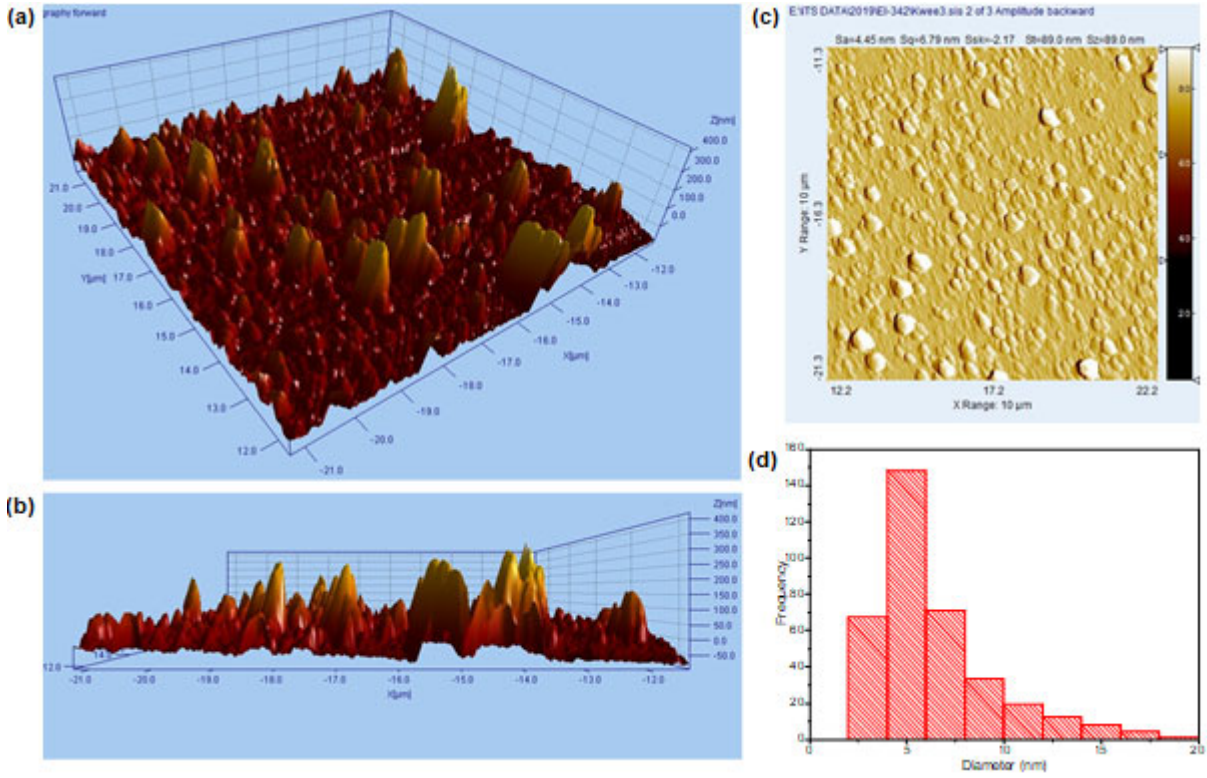

Fig 3. AFM photographs of Cat-CNDs on diagonal (a); vertical (b); top views (c); and its histogram (d)

as-synthesized CNDs solution. The height profile indicated that even though some particles had a size diameter of about 100 nm, the average size of these nanoparticles were about 5 nm supported by the histogram of the Cat-CNDs interpreted by the Image J software (Fig. 3(c)). Furthermore, it was revealed that the Cat-CNDs were well dispersed in the appropriate solvent and appeared in the spherical shape. The diameter of the CNDs was included in its size range which has been widely developed, which measures less than 10 nm in size [37].

Crystal characterization of the synthesized Cat-CNDs was investigated by XRD (Fig. 4). Its crystallinity was confirmed by a definite peak observed in the range of the shoulder diffractogram between 5 and 30°, confirming the peak of graphite carbon structure (based on crystal database JCPDS 74-2328). The XRD data also demonstrated interlayer spacing of Cat-CNDs on (003) plane at 11.15Å. The pyrolyzed CNDs performed weak XRD intensity, indicating nano-sized materials that matched with the supporting literature on nanostructure graphitic nature [38-39]. The average size of the crystalline CNDs with a 2θ position of 15.88 (FWHM = 7.2804°) was calculated to be 0.2 nm according to the Scherrer's equation.

Further observation focused on photo-physical properties of the CNDs that was acquired by using UV-Vis spectroscopy (Fig. 5(a)). The spectrum of pure catechin solution showed two absorption peaks that were

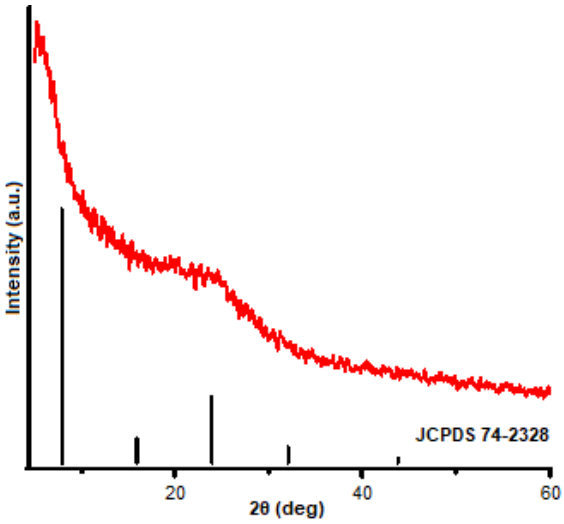

Fig 4. XRD pattern of Cat-CNDs

found at wavelengths of 267 and 318 nm corresponding to $\pi-\pi^*$ transitions of the aromatic ring. After the pyrolysis process, the synthesized Cat-CNDs possessed a nearly similar absorption spectrum to catechin. Furthermore, it was noticeable that two absorption peaks of Cat-CNDs appeared at around 267 nm, which was assigned to $\pi-\pi^*$, and 500 nm (blue shift emission) influencing electrostatic interactions between the aromatic rings within the catechin compound. The optical analysis of the as-prepared CNDs compared with bare catechin was further investigated (Fig. 5(b)). The data showed a strong fluorescent intensity presented as a broad peak (PL) at 500 nm, whereas pure catechin solution relatively exhibited a very weak fluorescent intensity centered at around 480 nm when both of the samples were exposed with excited wavelength at 380 nm (supported by the photograph in Fig. 5(b)). The photograph figures also show that Cat-CNDs had good solubility in water and hence having stronger fluorescence. For this reason, it was favorable for this material to be used as a staining agent for targeting tumor cells. Furthermore, it was noticed that the Cat-CNDs held excitation-dependent fluorescence on the complexity of the excited states of the CNDs, affecting the bandgap on the surface state of the carbon nanodots material [40].

Fig. 5(c) shows the Raman peak detected at 1590 cm^{-1} referring to a typical G band to the graphene (sp^2), due to the action of a double degenerated photo mode integrated with the symmetric E_{2g} in graphitic nature and the vibrations of the sp^2 were determined by the bonded carbon atoms in the two-dimension system of a hexagonal lattice [23]. The Raman data in Fig. 5(c) also show a peak at 1335 cm^{-1} described as the D band due to the disorder-induced nature in graphite of the sp^3 hybridization among carbon atoms which was inferred

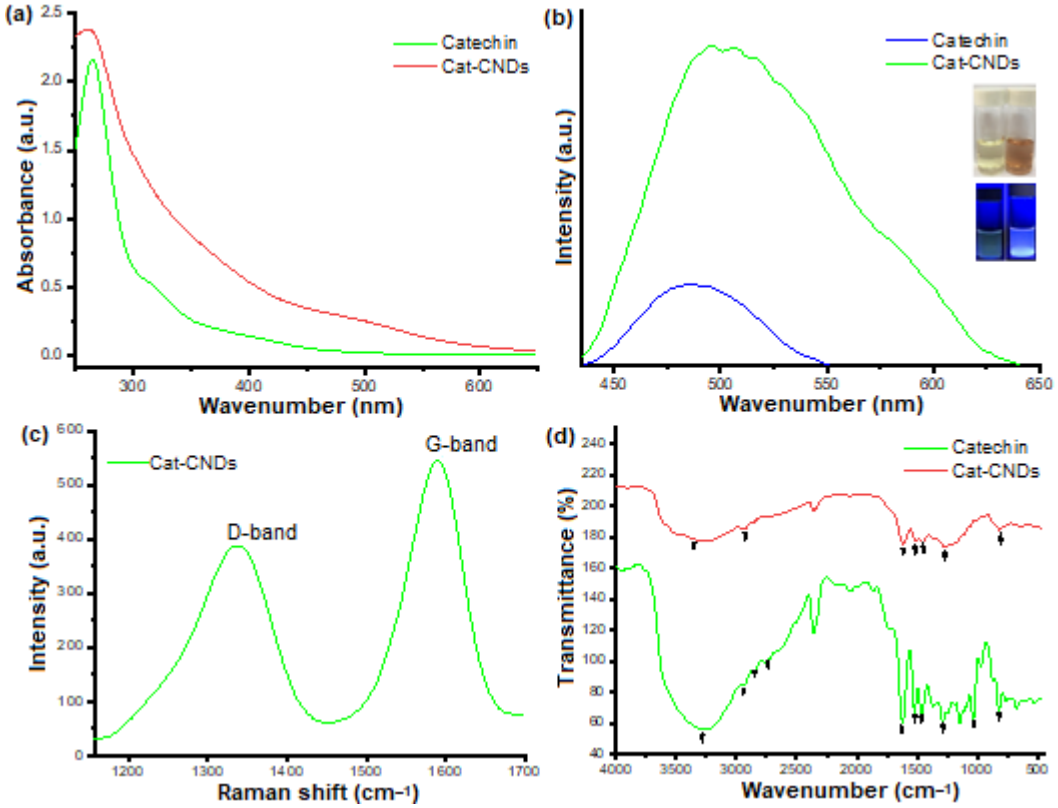

Fig 5. UV-Vis spectra of catechin (green solid line) and Cat-CNDs (red solid line) (a). PL spectra of catechin (blue solid line) and Cat-CNDs (red solid line). Inset: photographs of catechin and Cat-CNDs solutions under visible light and UV light (b). Raman spectra of Cat-CNDs (c). FTIR spectra of Cat-CNDs (red solid line) compared with bare Catechin (green solid line) (d)

to the A_{1g} mode [23]. These two bands are common bands of graphene or graphene oxide structure thus confirming the formation of a graphene oxide-like structure on the prepared Cat-CNDs. The calculation of the different intensity ratio of the D to G bands (I_D/I_G) resulted the value of 0.84, indicating the purity of graphitic formation. The CNDs sample with amorphous nature had a high ID/IG ratio whereas the CNDs sample with a high degree of graphitization was indicated by a relatively lower I_D/I_G ratio [41]. This means that the lower the intensity ratio of I_D/I_G, the more purified graphitic crystals were dominated. Therefore, the Raman spectrum confirmed a high purity of crystalline graphite in the carbon nanodots obtained from catechin.

As shown in Fig. 5(d), the functional groups of the Cat-CNDs were systemically analyzed with infra-red spectroscopy and compared with bare catechin.

For the catechin compound, a strong peak showed the stretching frequency of O–H bands at 3319 cm^{-1}, while C–H stretching of sp^2 hybridization was found at 2930 cm^{-1}, and C–H asymmetric and symmetric stretching vibrations of methane (–CH_2–) at 2871 and 2835 cm^{-1}, respectively. Furthermore, the bands between 1624 and 1525 cm^{-1} corresponded to the C=C stretching of the aromatic ring, while C–O/C–O–C stretching vibrations were found at 1285 cm^{-1} (symmetric band) and 1139 cm^{-1} (symmetric band), and C–H bending of CH_2 (out of plane) was found at 813 cm^{-1} [41]. In contrast the spectra for Cat-CNDs showed a broad peak at 3280 cm^{-1} that was attributed to the stretching vibration of a small number of residual hydroxyl groups that remained even after dehydrogenation, while the peak at 2926 cm^{-1} corresponded to C–H stretching vibration and aromatic ring stretching of the C=C vibration appeared at 1602, 1503, and 1450 cm^{-1}. The C–O–C stretching vibration was observed at 1280 cm^{-1}, and the broad peak at 810 cm^{-1} was attributed to the C=C–H out-of-plane bending. The synthesized carbon dots showed favorable hydrophilicity and good dispersion in water due to the polar functional groups on the surface site.

Stability Evaluation of Cat-CNDs

The colloidal stability analysis was carried out to assure the stability of Cat-CNDs. The stability of nanoparticles in aqueous solutions is vital for both biomedical and clinical uses. The first observation to study the pH effect on the CNDs, as shown in Fig. 6. The result showed that Cat-CNDs solution at pH 5 to 11 showed good stability up to 24 h after pH adjustment. However, Cat-CNDs at pH 3 and 4 showed precipitated particulates for the first 6 h. The change in appearance of the Cat-CNDs was observed at pH 12, where its color became bright brown. These conditions were likely due to the destruction of Cat-CNDs in extreme conditions. At low pH, the hydroxyl-abundant environment most likely caused the increase of hydrogen bonding of the CNDs [43], whereas structural destruction occurred when the CNDs were treated in high pH resulting in the color change. These findings were supported by UV-Vis spectra analysis (Fig. 6(b)), where π^*–π excitation of CNDs at wavelength below 300 nm was disrupted by its electrostatic effect.

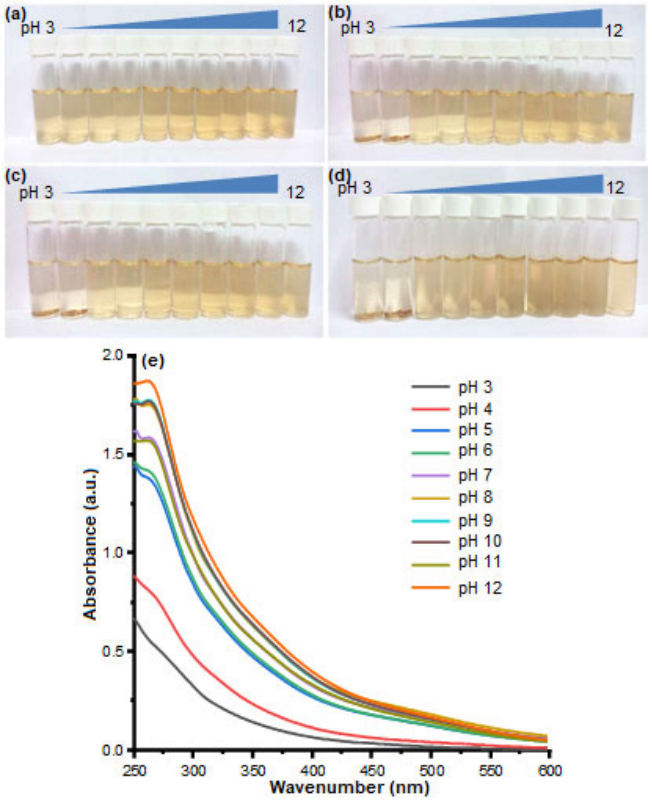

Fig 6. Photograph images of Cat-CNDs from pH 3 to pH 12 at (a) 0 h, (b) 6 h, (c) 12 h, and (d) 24 h. (e) The UV-Vis Spectra of Cat-CNDs from pH 3 to pH 12

The stability of CNDs was then observed against varied thermal treatment (30–100 °C). As a result, in Fig. 7(a), there were no coagulation and color change, while UV-Vis spectroscopy analysis revealed that all of the varied CNDs resulted similar absorption spectra. The synthesis of Cat-CNDs that reached up to 270 °C produced good thermal stability of this material and fulfilled the thermal stability requirement for materials that can be applied for the human body.

Further assessment was focused on Cat-CNDs stability on varied ionic strength by NaCl addition. This part was considered necessary due to the blood circulation in the human body that is affected by salt concentration. Thus, the effect of ionic strength on prepared Cat-CNDs was a crucial factor for further clinical applications. As shown in Fig. 8(a), the CNDs mixed with varying concentrations of NaCl salts (from 0.1 to 0.5 M) show similar conditions with the untreated Cat-CNDs, showing no coagulated solids even until 24 h.

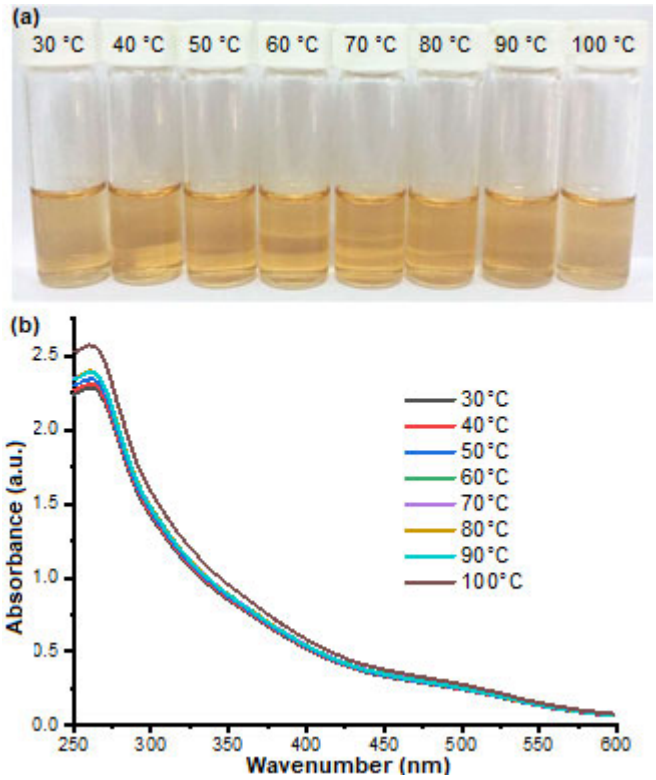

Fig 7. Photograph of Cat-CNDs on varied temperature assessment at 30, 40, 50, 60, 70, 80, 90, and 100 °C (a), The UV-Vis spectra of Cat-CNDs at varied temperatures treatment after 24 h (b)

This data is supported by the UV-Vis spectra (Fig. 8(e)), where the maximum wavelengths of the treated CNDs were similar to the untreated Cat-CNDs. Therefore, all these stability investigations prove the potential of this material for bio-applications and other fields of commercial purpose.

Confocal Observation

The fluorescence properties possessed by Cat-CNDs were the main factor to consider applying this material for tumor cell staining. Laser confocal scanning microscopy (LCSM) was used to improve the fluorescent properties as well as the cellular uptake and internalization of Cat-CNDs on the HeLa tumor cell. After 4 h of addition and incubation of Cat-CNDs onto HeLa (Fig. 9), its green emission was detected and localized in the cytoplasm of Hela tumor cells. This finding

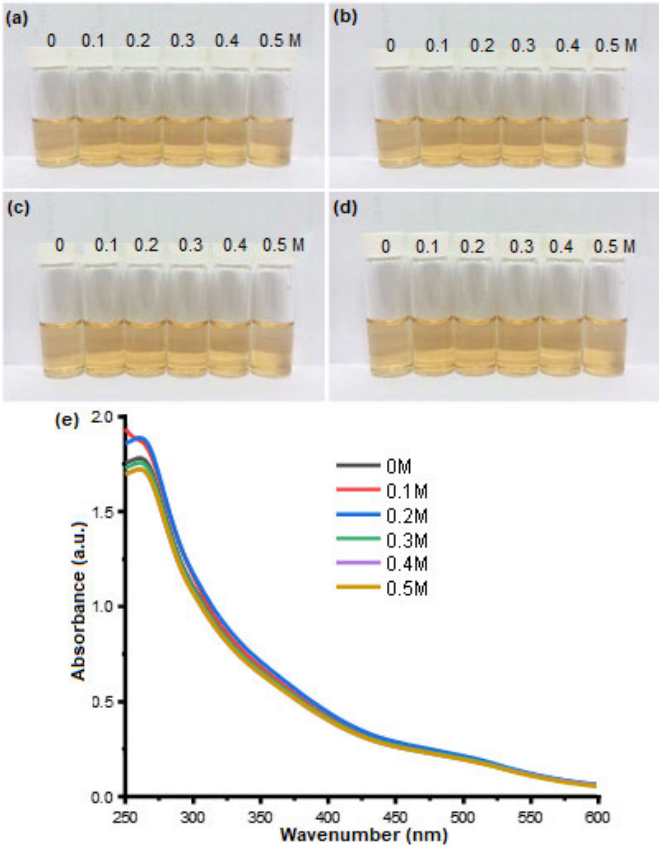

Fig 8. Photograph images of Cat-CNDs on varied NaCl concentration at 0 h (a), 6 h (b), 12 h (c), and 24 h (d). The UV-Vis spectra of Cat-CNDs at varied concentrations of NaCl after 24 h (e)

indicates that CNDs were successfully taken up by the cells.

The facile internalization of CNDs on the tumor cell was considered based on the basic properties of the catechin compound that possess high affinities to a variety of proteins expressed on the cell membrane by massive hydrogen bonding [44-45]. Further reports also stated that the insertion of catechin was founded by an association of membrane plasma by lipid rafts [46]. We speculate to that those reasons made the Cat-CNDs significantly appear on the cytoplasm. To ensure the position of Cat-CNDs on the cytoplasm, the Z stacking mode of CLSM was used (Fig. 10), where higher emission of the cell was found in the middle position. Therefore, these findings proved the potential and biocompatibility of Cat-CNDs while staining on a specific tumor cell and showed similar results with a previous report [46].

Cytotoxicity Test with CCK-8 Assay

Several studies have reported the anticancer potential of catechin derivatives, including the cytotoxicity of catechin when it is modified to nanoparticle form, which is an important aspect to verify its biocompatibility in biomedical and pharmaceutical applications. The cytotoxicity evaluation is conducted by

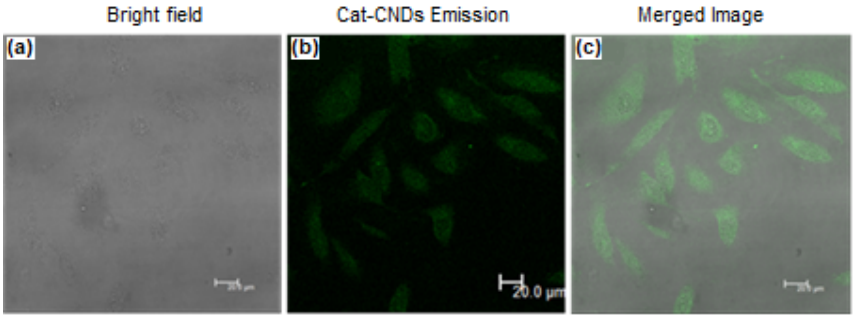

Fig 9. CLSM images of HeLa tumor cell after 4 h incubation with Cat-CNDs

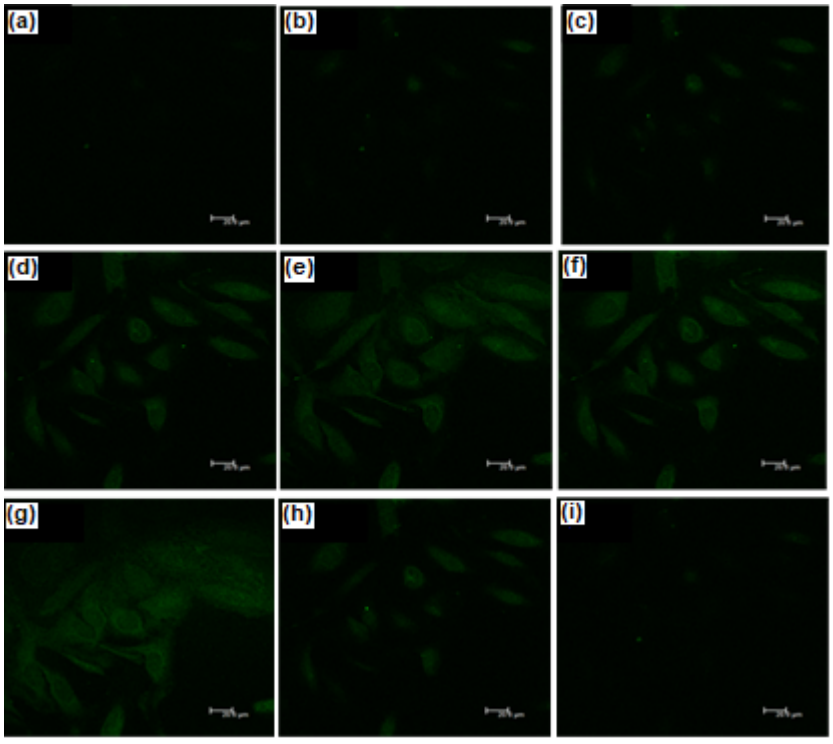

Fig 10. CLSM images of HeLa cells through z-stacking mode after 4 h treated with Cat-CNDs (a-i) Hela cells images captured by excitation at 488 nm

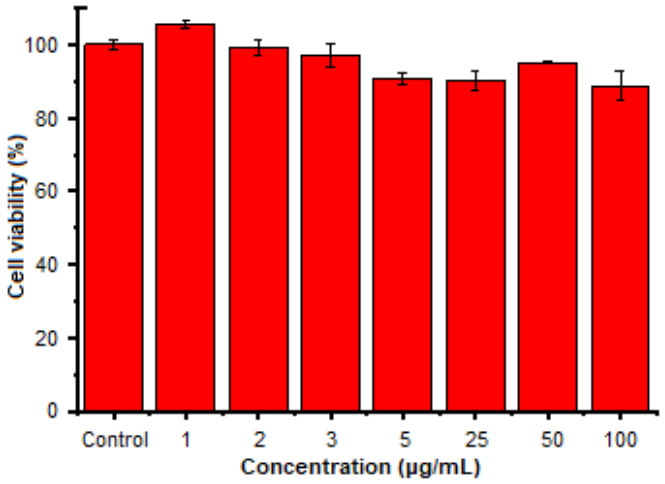

Fig 11. Cell viability assessed byWST-8 assay of Hela Cells after 24 h of treatment with Cat-CNDs. WST-8 data is shown as means ± SD with n = 3

incubating the adjusted concentration of Cat-CNDs on HeLa cells via WST-8 assay (Fig. 11). After being incubated for 24 h, the cell viability results showed that the cell had a high viability percentage of over 80% in concentrations of up to 400 µg mL^{-1} and IC_{50} of about 1815 µg mL^{-1}. This strongly indicated that Cat-CNDs have very low toxicity. Previous reports show that synthesized carbon nanodots are classified into non-toxic and low toxic categories if the percentage of cell viability is between 50.0–80.0% [47-48].

■ CONCLUSION

Catechin was successfully isolated from *Uncaria gambir* as raw material for the synthesis of Cat-CNDs through a single-step pyrolysis method and was later used for staining specific tumor cells. The resulting Cat-CNDs possess excellent optical properties. The average size of the Cat-CNDs was found to be below 5 nm with near-spherical shape and was crystalline in nature, which was confirmed by the analysis of the physicochemical properties. Moreover, the Cat-CNDs could be easily internalized into the tested Hela cancer cells and demonstrated excellent biocompatibility without any obvious toxicity. Due to their good biocompatibility, non-toxicity, strong photoluminescence, and eco-friendliness; this work strongly suggested that the as-synthesized Cat-CNDs have much potential to be applied for various biomedical applications specifically in targeted staining of specific tumor cells.

■ ACKNOWLEDGMENTS

Authors would like to thank Universitas Airlangga, Indonesia for research facilities and funding under contract 341/UN3.14/LT/2019.

■ REFERENCES

[1] Nandika, D., Syamsu, K., Arinana, A., Kusumawardani, D.T., and Fitriana, Y., 2019, Bioactivities of catechin from Gambir (*Uncaria gambir* Roxb.) against wood-decaying fungi, *BioResources*, 14 (3), 5646–5656.

[2] Davis, A.P., and Figueiredo, E., 2007, A checklist of the Rubiaceae (coffee family) of Bioko and Annobon (Equatorial Guinea, Gulf of Guinea), *Syst. Biodivers.*, 5 (2), 159–186.

[3] Anggraini, T., Tai, A., Yoshino, T., and Itani, T., 2011, Antioxidative activity and catechin content of four kinds of *Uncaria gambir* extract from West Sumatra, Indonesia, *Afr. J. Biochem. Res.*, 5 (1), 33–38.

[4] Amir, M., Mujeeb, M., Khan, A., Ashraf, K., Sharma, D., and Aqil, M., 2012, Phytochemical analysis and *in vitro* antioxidant activity of *Uncariagambir*, *Int. J. Green Pharm.*, 6 (1), 67–72.

[5] Ahmad, R., Hashim, H.M., Noor, Z.M., Ismail, N.H., Salim, F., Lajis, N.H., and Shaari, K., 2011, The Antioxidant and antidiabetic potential activity of Malaysian *Uncaria*, *Res. J. Med. Plant*, 5 (5), 587–595.

[6] Picking, D., Delgoda, R., Boulogne, I., and Mitchell, S., 2013, *Hyptis verticillata* Jacq: A review of its traditional uses extension, phytochemistry, pharmacology, and toxicology, *J. Ethnopharmacol.*, 147 (1), 16–41.

[7] Heitzman, M.E., Neto, C.C., Winiarz, E.,Vaisberg, A.J., and Hammond, G.B., 2005, Ethnobotany, phytochemistry, and pharmacology of *Uncaria* (Rubiaceae), *Phytochemistry*, 66 (1), 5–29.

[8] Gadkari, P.V., and Balaraman, M., 2015, Catechins: Sources, extraction, and encapsulation: A review, *Food Bioprod. Process.*, 93, 122–138.

[9] Zhang, Q., Zhao, J.J., Xu, J., Feng, F., and Qu, W., 2015, Medicinal uses, phytochemistry and pharmacology of the genus *Uncaria gambir*, *J. Ethnopharmacol.*, 173, 48–80.

[10] Melia, S., Novia, D., and Juliyarsi, I., 2015, Antioxidant and antimicrobial activities of gambir (*Uncaria gambir* Roxb) extracts and their application in *rendang*, *Pak. J. Nutr.*, 14 (12), 938–941.

[11] Ferdinal, N., 2014, A simple purification method of catechin from gambier, *IJASEIT*, 4 (6), 53–55.

[12] Fujiwara, H., Takayama, S., Iwasaki, K., Tabuchi, M., Yamaguchi, T., Sekiguchi, K., Ikarashi, Y., Kudo, Y., Kase, Y., Arai, H., and Yaegashi, N., 2011, Yokukansan, a traditional Japanese medicine, ameliorates memory disturbance and abnormal social interaction with anti-aggregation effect of cerebral amyloid β proteins in amyloid precursor protein transgenic mice, *Neuroscience*, 180, 305–313.

[13] Mizukami, K., Asada, T., Kinoshita, T., Tanaka, K., Sonohara, K., Nakai, R., Yamaguchi, K., Hanyu, H., Kanaya, K., Takao, T., Okada, M., Kudo, S., Kotoku, H., Iwakiri, M., Kurita, H., Miyamura, T., Kawasaki, Y., Omori, K., Shiozaki, K., Odawara, T., Suzuki, T., Yamada, S., Nakamura, Y., and Toba, K., 2009, A randomized cross-over study of a traditional Japanese medicine (kampo), yokukansan, in the treatment of the behavioural and psychological symptoms of dementia, *Int. J. Neuropsycho. Pharmacol.*, 12 (2), 191–199.

[14] Shen, J., Zhu, Y., Yang, X., and Li, C., 2012, Graphene quantum dots: Emergent nanolights for bioimaging, sensors, catalysis, and photovoltaic devices, *Chem. Commun.*, 48 (31), 3686–3699.

[15] Wang, X., Cao, L., Yang, S.T., Lu, F., Meziani, M.J., Tian, L., Sun, K.W., Bloodgood, M.A., and Sun, Y.P., 2010, Bandgap-like strong fluorescence in functionalized carbon nanoparticles, *Angew. Chem. Int. Ed.*, 49, 5310–5314.

[16] Sun, Y.P., Wang, X., Lu, F., Cao, L., Meziani, M.J., Luo, P.G., Gu, L., and Veca, L.M., 2008, Doped carbon nanoparticles as a new platform for highly photoluminescent dots, *J. Phys. Chem. C*, 112 (47), 18295–18298.

[17] Vandarkuzhali, S.A., Jeyalakshmi, V., Sivaraman, G., Singaravadivel, S., Krishnamurthy, K.R., and Viswanathan, B., 2017, Highly fluorescent carbon dots from pseudo-stem of banana plant: Applications as nanosensor and bio-imaging agents, *Sens. Actuators, B*, 252, 894–900.

[18] Namdari, P., Negahdari, B., and Eatemadi, A., 2017, Synthesis, properties and biomedical applications of carbon-based quantum dots: An updated review, *Biomed. Pharmacother.*, 87, 209–222.

[19] Zhang, Q., Xie, S., Yang, Y., Wu, Y., Wang, X., Wu, J., Zhang, L., Chen, J., and Wang, Y., 2018, A facile synthesis of highly nitrogen-doped carbon dots for imaging and detection in biological samples, *J. Anal. Methods Chem.*, 2018, 7890937.

[20] Himaja, A.L., Karthik, P.S., Sreedhar, B., and Singh, S.P., 2014, Synthesis of carbon dots from kitchen waste: Conversion of waste to value added product, *J. Fluoresc.*, 24 (6), 1767–1773.

[21] Das, R., Bandyopadhyay, R., and Pramanik, P., 2018, Carbon quantum dots from natural resource: A review, *Mater. Today Chem.*, 8, 96–109.

[22] Baguley, D.M., Humphriss, R.L., Axon, P.R., and Moffat, D.A., 2005, Change in tinnitus handicap after translabyrinthine vestibular schwannoma excision, *Otol. Neurotol.*, 26 (5), 1061–1063.

[23] Yallappa, S., Manaf, S.A.A., and Hegde, G., 2018, Synthesis of a biocompatible nanoporous carbon and its conjugation with florescent dye for cellular imaging and targeted drug delivery to cancer cells, *New Carbon Mater.*, 33 (2), 162–172.

[24] Wang, J., Cheng, C., Huang, Y., Zheng, B., Yuan, H., Bo, L., Zheng, M.W., Yang, S.Y., Guo, Y., and Xiao, D., 2014, A facile large-scale microwave synthesis of highly fluorescent carbon dots from benzenediol isomers, *J. Mater. Chem. C*, 2 (25), 5028–5035.

[25] Xiao, F.X., Miao, J., and Liu, B., 2014, Layer-by-layer self-assembly of CdS quantum dots/graphene nanosheets hybrid films for photoelectrochemical and photocatalytic applications, *J. Am. Chem. Soc.*, 136 (4), 1559–1569.

[26] Fahmi, M.Z., Sukmayani, W., Khairunisa, S.Q., Witaningrum, A.M., Indriati, D.W., Matondang,

M.Q.Y., Chang, J.Y., Kotaki, T., and Kameoka, M., 2016, Design of boronic acid-attributed carbon dots on inhibits HIV-1 entry, *RSC Adv.*, 6 (95), 92996–93002.

[27] Thoo, L., Fahmi, M.Z., Zulkipli, I.N., Keasberry, N., and Idris, A., 2017, Interaction and cellular uptake functions of surface-modified carbon dot nanoparticles by J774. 1 macrophages, *Cent. Eur. J. Immunol.*, 42 (3), 324–330.

[28] Yao, J., Feng, J., and Chen, J., 2016, External-stimuli responsive systems for cancer theranostic, *Asian J. Pharm. Sci.*, 11 (5), 585–595.

[29] Saneja, A., Kumar, R., Arora, D., Kumar, S., Panda, A.K., and Jaglan, S., 2018, Recent advances in near-infrared light-responsive nanocarriers for cancer therapy, *Drug Discovery Today*, 23 (5), 1115–1125.

[30] Xu, W., Qian, J., Hou, G., Suo, A., Wang, Y., Wang, J., Sun, T., Yang, M., Wan, X., and Yao, Y., 2017, Hyaluronic acid-functionalized gold nanorods with pH/NIR dual-responsive drug release for synergetic targeted photothermal chemotherapy of breast cancer, *ACS Appl. Mater. Interfaces*, 9 (42), 36533–36547.

[31] Huang, C.Y., Ju, D.T., Chang, C.F., Reddy, P.M., and Velmurugan, B.K., 2017, A review on the effects of current chemotherapy drugs and natural agents in treating non–small cell lung cancer, *BioMedicine*, 7 (4), 23.

[32] Feng, T., Ai, X., An, G., Yang, P., and Zhao, Y., 2016, Charge-convertible carbon dots for imaging-guided drug delivery with enhanced in vivo cancer therapeutic efficiency, *ACS Nano*, 10 (4), 4410–4420.

[33] Fahmi, M.Z., Chen, J.K., Huang, C.C., Ling, Y.C., and Chang, J.Y., 2015, Phenylboronic acid-modified magnetic nanoparticles as a platform for carbon dot conjugation and doxorubicin delivery, *J. Mater. Chem. B*, 3 (27), 5532–5543.

[34] Yan, T., Zhong, W., Yu, R., Yi, G., Liu, Z., Liu, L., Wang, X., and Jiang, J., 2019, Nitrogen-doped fluorescent carbon dots used for the imaging and tracing of different cancer cells, *RSC Adv.*, 9 (43), 24852–24857.

[35] Fahmi, M.Z., Haris, A., Permana, A.J., Wibowo, D.L.N., Purwanto, B., Nikmah, Y.L., and Idris, A., 2018, Bamboo leaf-based carbon dots for efficient tumor imaging and therapy, *RSC Adv.*, 8 (67), 38376–38383.

[36] Acharya, P.P., Genwali, G.R., and Rajbhandari, M., 2013, Isolation of catechin from *Acacia catechu* willdenow estimation of total flavonoid content in *Camellia sinensis* Kuntze and *Camellia sinensis* Kuntze var. *assamica* collected from different geographical region and their antioxidant activities, *Sci. World*, 11 (11), 32–36.

[37] Bhunia, S.K., Saha, A., Maity, A.R., Ray, S.C., and Jana, N.R., 2013, Carbon nanoparticle-based fluorescent bioimaging probes, *Sci. Rep.*, 3, 1473.

[38] Saravanan, K.R.A., Prabu, N., Sasidharan, M., and Maduraiveeran, G., 2019, Nitrogen-self doped activated carbon nanosheets derived from peanut shells for enhanced hydrogen evolution reaction, *Appl. Surf. Sci.*, 489, 725–733.

[39] Fei, H., Li, H., Li, Z., Feng, W., Liu, X., and Wei, M., 2014, Facile synthesis of graphite nitrate-like ammonium vanadium bronzes and their graphene composites for sodium-ion battery cathodes, *Dalton Trans.*, 43 (43), 16522–16527.

[40] Choi, J., Kim, N., Oh, J.W., and Kim, F.S., 2018, Bandgap engineering of nanosized carbon dots through electron-accepting functionalization, *J. Ind. Eng. Chem.*, 65, 104–111.

[41] Huang, C.C., Hung, Y.S., Weng, Y.M., Chen, W., and Lai, Y.S., 2019, Sustainable development of carbon nanodots technology: Natural products as a carbon source and applications to food safety, *Trends Food Sci. Technol.*, 86, 144–152.

[42] Sepperer, T., and Tondi, G., 2018, Fractioning of Industrial Tannin Extract in Different Organic Solvents, *Das 12. Forschungs forum der österreichischen Fachhochschulen (FFH)*, 4–5 April 2018, Campus Urstein, Salzburg, Austria.

[43] Jia, X., Li, J., and Wang, E., 2012, One-pot green synthesis of optically pH-sensitive carbon dots with up conversion luminescence, *Nanoscale*, 4 (18), 5572–5575.

[44] Rawangkan, A., Wongsirisin, P., Namiki, K., Iida, K., Kobayashi, Y., Shimizu, Y., Fujiki, H., and

Suganuma, M., 2018, Green tea catechin is an alternative immune checkpoint inhibitor that inhibits PD-L1 expression and lung tumor growth, *Molecules*, 23 (8), E2071.

[45] Yang, C.S., and Wang, H., 2016, Cancer preventive activities of tea catechins, *Molecules*, 21 (12), E1679.

[46] Negri, A., Naponelli, V., Rizzi, F., and Bettuzzi, S., 2018, Molecular targets of epigallocatechin—Gallate (EGCG): A special focus on signal transduction and cancer, *Nutrients*, 10 (12), E1936.

[47] Fahmi, M.Z., Wibowo, D.L.N., Sakti, S.C.W., Lee, H.V., and Isnaeni, 2020, Human serum albumin capsulated hydrophobic carbon nanodots as staining agent on HeLa tumor cell, *Mater. Chem. Phys.*, 239, 122266.

[48] Ansari, A.A., Hasan, T., Syed, N., Labis, J., and Alshatwi, A.A., 2017, *In-vitro* cytotoxicity and cellular uptake studies of luminescent functionalized core-shell nanospheres, *Saudi J. Biol. Sci.*, 24 (6), 1392–1403.